Eur. Phys. J. A (2016) **52**: 74
DOI 10.1140/epja/i2016-16074-5

THE EUROPEAN PHYSICAL JOURNAL A

Regular Article – Experimental Physics

Primordial nucleosynthesis*

C. Gustavino[1], M. Anders[2,3,a], D. Bemmerer[2], Z. Elekes[4], and D. Trezzi[5,b]

[1] INFN, Sezione di Roma La Sapienza, Piazzale A. Moro 2, 00185 Roma, Italy
[2] Helmholtz-Zentrum Dresden-Rossendorf, Bautzner Landstr. 400, 01328 Dresden, Germany
[3] Technische Universität Dresden, Mommsenstrasse 9, 01069 Dresden, Germany
[4] Institute for Nuclear Research of the Hungarian Academy of Sciences (MTA Atomki), Bem tér 18/c., Debrecen, Hungary
[5] Università degli Studi di Milano and INFN, Sezione di Milano, Via Celoria 16, 20133 Milano, Italy

Received: 23 August 2015 / Revised: 23 December 2015
Published online: 5 April 2016 –
Communicated by C. Broggini

Abstract. Big Bang nucleosynthesis (BBN) describes the production of light nuclei in the early phases of the Universe. For this, precise knowledge of the cosmological parameters, such as the baryon density, as well as the cross section of the fusion reactions involved are needed. In general, the energies of interest for BBN are so low ($E < 1\,\mathrm{MeV}$) that nuclear cross section measurements are practically unfeasible at the Earth's surface. As of today, LUNA (Laboratory for Underground Nuclear Astrophysics) has been the only facility in the world available to perform direct measurements of small cross section in a very low background radiation. Owing to the background suppression provided by about 1400 meters of rock at the Laboratori Nazionali del Gran Sasso (LNGS), Italy, and to the high current offered by the LUNA accelerator, it has been possible to investigate cross sections at energies of interest for Big Bang nucleosynthesis using protons, ^{3}He and alpha particles as projectiles. The main reaction studied in the past at LUNA is the $^2\mathrm{H}(^4\mathrm{He},\gamma)^6\mathrm{Li}$. Its cross section was measured directly, for the first time, in the BBN energy range. Other processes like $^2\mathrm{H}(\mathrm{p},\gamma)^3\mathrm{He}$, $^3\mathrm{He}(^2\mathrm{H},\mathrm{p})^4\mathrm{He}$ and $^3\mathrm{He}(^4\mathrm{He},\gamma)^7\mathrm{Be}$ were also studied at LUNA, thus enabling to reduce the uncertainty on the overall reaction rate and consequently on the determination of primordial abundances. The improvements on BBN due to the LUNA experimental data will be discussed and a perspective of future measurements will be outlined.

1 Introduction: Astrophysical motivation

The Big Bang nucleosynthesis (BBN) theory describes the formation of light nuclides in the first minutes of cosmic time, as the result of the competition between the rapidly expanding Universe and the reaction rate of relevant nuclear processes [1,2]. In standard cosmology, the expansion rate of the universe is governed by the Friedmann equation,

$$H^2 = \frac{8\pi}{3} G\rho, \tag{1}$$

where H is the Hubble parameter, G is the Newton gravitational constant and ρ is the energy density which, in the early Universe, is dominated by "radiation", *i.e.* the contributions from massless or extremely relativistic particles. The only known relativistic particles at the BBN epoch are the photons (with $g_\gamma = 2$ degrees of freedom or helicities) and the three neutrino families (with $g_\nu = 2$, taking into account left-handed neutrinos and right-handed antineutrinos). Therefore, the radiation density can be expressed as follows:

$$\rho = \rho_\gamma \left[1 + \frac{7}{8}\left(\frac{4}{11}\right)^{4/3} N_{\mathrm{eff}}\right]. \tag{2}$$

In this formula ρ_γ is the photon density and N_{eff} is the contribution of other relativistic species. Using this formula $N_{\mathrm{eff}} = 3.046$ if only the three known neutrino families are considered.

As shown in fig. 1, the nucleosynthesis begins with the formation of deuterium by $\mathrm{p}(\mathrm{n},\gamma)^2\mathrm{H}$ reaction. Because of the large density of photons (the baryon-to-photon ratio is $\eta = 6 \times 10^{-10}$), the photo-dissociation delays the production of deuterium well after the temperature T drops below the binding energy of deuterium ($Q = 2.23\,\mathrm{MeV}$). Subsequently, ^{3}H and ^{3}He are produced via the $^2\mathrm{H}(^2\mathrm{H},\mathrm{p})^3\mathrm{H}$, $^2\mathrm{H}(^2\mathrm{H},\mathrm{n})^3\mathrm{He}$ and $^2\mathrm{H}(\mathrm{p},\gamma)^3\mathrm{He}$ processes.

* Contribution to the Topical Issue "Underground nuclear astrophysics and solar neutrinos: Impact on astrophysics, solar and neutrino physics" edited by Gianpaolo Bellini, Carlo Broggini, Alessandra Guglielmetti.

[a] *Present address*: Sächsisches Staatministerium für Umwelt und Landwirtschaft, Dresden, Germany.
[b] e-mail: davide.trezzi@mi.infn.it

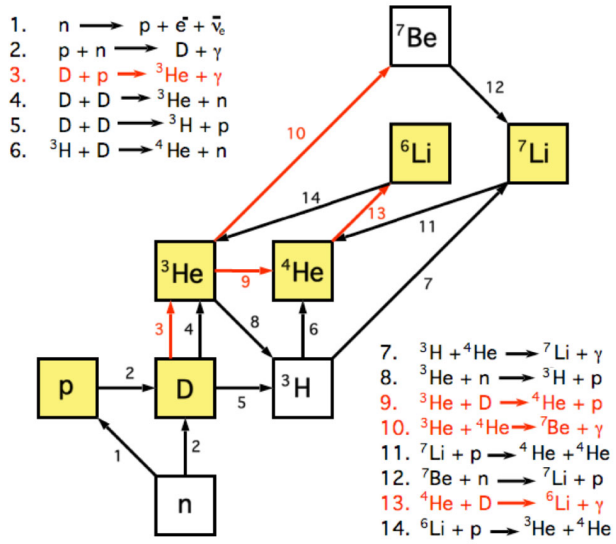

Fig. 1. Leading processes of Big Bang nucleosynthesis. Yellow boxes mark stable isotopes. The nuclear processes studied by LUNA are highlighted in red.

Finally, the ^{3}H(^{2}H, n)^{4}He and ^{3}He(^{2}H, p)^{4}He reactions produce ^{4}He, in which nearly all the free neutrons end up bound, while the abundances of deuterium, tritium and ^{3}He are relatively small (residual tritium is successively converted into ^{3}He via weak decay). The primordial abundance of heavier isotopes ^{7}Li and ^{6}Li is even smaller (after BBN, the produced ^{7}Be decays into ^{7}Li), because the absence of stable nuclei with mass number 5 impedes nucleosynthesis via $^4\mathrm{He} + \mathrm{n}$ and $^4\mathrm{He} + \mathrm{p}$ reactions. Finally, the production of nuclides with $A > 8$ is negligible, because the lack of stable nuclei with $A = 8$ prevents nuclear reactions through the $^4\mathrm{He} + {}^4\mathrm{He}$ channel to occur.

In the ΛCDM model (*i.e.* the standard model of Big Bang cosmology), the only free parameter is the baryon density, usually expressed normalized to the black-body photon density as $\eta = \mathrm{n}_B/\mathrm{n}_\gamma$. While both densities change with time and temperature, their ratio remains constant from the end of BBN to the present. Because standard BBN is a one-parameter theory, the comparison between any abundance measurement with the BBN calculation determines η, while additional measurements overconstrain the theory and thereby provide a consistency check. Incidentally, the η parameter has been recently derived with high accuracy by the Cosmic Microwave Background (CMB) experiments [3]. Consequently, using such a η_{CMB} value as a fixed parameter in the ΛCDM model it is possible to let the light element abundances free to vary. In this case, the primordial abundances are thus completely determined within the CMB and BBN uncertainties. The obtained results have to be compared with the direct observations for light isotopes in the Universe. As a general method, the primordial abundance is then derived by extrapolating to zero metallicity the amount of light isotopes observed in metal-poor and/or faraway sites, where the abundances are thought to be less polluted by processes like stellar burning and cosmic-ray interactions.

Table 1. Calculated and observed abundances of light isotopes derived from standard BBN and from direct astrophysical observations (see text). In this table, the primordial ^{4}He abundance is given in terms of the baryon mass fraction Y_p, *i.e.* the ratio between helium and baryon densities at that time. The abundance of the other nuclides is expressed by ratios.

Isotope	SBBN theory	Observations
Y_p	0.24771 ± 0.00014 [3]	0.254 ± 0.003 [4]
D/H	$(2.6 \pm 0.07) \times 10^{-5}$ [3]	$(2.53 \pm 0.04) \times 10^{-5}$ [5]
^{3}He/H	$(1.00 \pm 0.01) \times 10^{-5}$ [6]	$(0.9 \pm 1.3) \times 10^{-5}$ [7]
^{7}Li/H	$(4.68 \pm 0.67) \times 10^{-10}$ [6]	$(1.23^{+0.68}_{-0.32}) \times 10^{-10}$ [8]
^{6}Li/^{7}Li	$(1.5 \pm 0.3) \times 10^{-5}$ [9]	$\lesssim 10^{-2}$ [10]

Table 1 summarizes both the results of BBN calculations (assuming the ΛCDM model and the η parameter derived from CMB experiments) and the results of direct observations for light isotopes.

As stated above, the computed ^{4}He abundance essentially depends on the amount of free neutrons available, therefore its (very small) uncertainty is almost entirely due to the neutron lifetime error [1,2]. The primitive abundance of ^{4}He derived from observations is deduced from observations in HII (ionized hydrogen) regions of compact blue galaxies. The uncertainty is mainly due to systematics such as plasma temperature or stellar absorption [4]. It is worth pointing out that the abundance of helium strongly depends on the expansion rate of the Universe. As a matter of fact, the faster the expansion is, the faster is the cooling. As a consequence, the BBN inset starts earlier, when the amount of neutrons available to form ^{4}He is higher. Therefore, the comparison between observed and calculated amount of helium depends on N_{eff} (see eqs. (1) and (2)), thus constraining the possible existence of "dark radiation", *i.e.* extra relativistic species in the early Universe not considered in the ΛCDM model.

Apart from helium, the calculated abundances of all the other nuclides strongly depend on the details of the BBN reaction chain [1,2]. As it will be shown in the next sections, the error budget of theoretical abundances has been remarkably improved by the LUNA experiment through the cross section measurement of the $^2\mathrm{H}(\mathrm{p},\gamma)^3\mathrm{He}$ [11], $^3\mathrm{He}(^2\mathrm{H},\mathrm{p})^4\mathrm{He}$ [12,13], $^3\mathrm{He}(^4\mathrm{He},\gamma)^7\mathrm{Be}$ [14–17] and $^2\mathrm{H}(^4\mathrm{He},\gamma)^6\mathrm{Li}$ [9] processes.

The abundance of deuterium is of particular importance because recent works in Damped Lyman-Alpha (DLA) systems at high redshifts provide the primordial abundance of deuterium with good accuracy [5]. As shown in table 1, the error of $(\mathrm{D/H})_{\mathrm{BBN}}$ is higher than the $(\mathrm{D/H})_{\mathrm{OBS}}$ one, calling for a renewed measurement of the $^2\mathrm{H}(\mathrm{p},\gamma)^3\mathrm{He}$ process [18]. As the deuterium abundance strongly depends on the baryon density, the comparison of $(\mathrm{D/H})_{\mathrm{BBN}}$ and $(\mathrm{D/H})_{\mathrm{OBS}}$ allows to measure the

η parameter (at the BBN epoch) with about the same accuracy of the one derived from CMB experiments. The (D/H) value is also sensitive to the expansion rate of universe, therefore it can be exploited to constrain the existence of "dark radiation", in combination with the ^{4}He results [5,19] or with CMB experiments [3,18].

The $(^3\mathrm{He/H})_{\mathrm{BBN}}$ value has a quite small error. Unfortunately, the ^{3}He observations in our galaxy are affected by large systematical uncertainties because this isotopes is both produced and destroyed in stars so that its primordial amount is quite uncertain [7]. Therefore, up to now ^{3}He does not represent a powerful probe to constrain the ΛCDM model.

The abundance of $^7\mathrm{Li/H_{OBS}}$ is deduced from the strength of its characteristic absorption line at about 680 nm in low metallicity stars in the galactic halo. The observations show that the lithium abundance is almost independent of metallicity (Spite plateau [20]).

This asymptotic value is interpreted as the primordial ^{7}Li abundance pointing out the tension between observations and theory, referred in literature as the "lithium problem".

Finally, concerning the ^{6}Li isotope, a controversial measurement is reported in the literature where the ^{6}Li abundance is obtained from the analysis of metal poor stars absorption spectra [10]. Even though many of the claimed ^{6}Li detections are questionable, for a very few metal-poor stars there still seems to be a significant amount of ^{6}Li ("the second lithium problem") [21].

The ^{6}Li abundance error has been recently reduced with the measurement of the cross section of the $^2\mathrm{H}(^4\mathrm{He},\gamma)^6\mathrm{Li}$ process at BBN energies by the LUNA experiment.

In summary, the BBN theory provides a powerful tool to constrain particle physics and cosmology. Although primordial abundances span many orders of magnitude, it is quite impressive that observations and theory are fairly in agreement, thus confirming the overall validity of standard BBN. However, some inconsistency between theory and measurements is apparent, possibly due to physics beyond the Standard Model (concerning the theoretical predictions) or to the lack of knowledge of astrophysical processes (concerning the abundances derived from direct observations). As an example, the existence of extra relativistic species beside photons and standard neutrinos increases Y_p and (D/H) [5,19], while the abundance of lithium isotopes can be affected by new physics, such as the existence of supersymmetric particles at the BBN epoch [22–25]. Although the impressive improvements in nuclear astrophysics reached in the last years, the present "precision cosmology" era is calling for a renewed study of the relevant nuclear processes in order to understand cosmology and particle physics in a coherent way.

2 The BBN fusion reactions investigated at LUNA

In this section, the improvements on BBN due to LUNA data will be discussed in details.

2.1 $^2\mathrm{H}(\mathrm{p},\gamma)^3\mathrm{He}$

Big Bang nucleosynthesis (BBN) started when the temperature of the Universe was low enough to break the equilibrium between deuteron production through $\mathrm{p(n},\gamma)^2\mathrm{H}$ and photo-disassociation through $^2\mathrm{H}(\gamma,\mathrm{n})\mathrm{p}$ (the so-called "deuterium bottleneck"). Owing to the environmental temperature of the order of GK and the huge amount of protons present at that time, ^{3}He was created through the $^2\mathrm{H}(\mathrm{p},\gamma)^3\mathrm{He}$ and $^2\mathrm{H}(^2\mathrm{H},\mathrm{n})^3\mathrm{He}$ reactions. At the same time these two reactions, together with the $^2\mathrm{H}(^2\mathrm{H},\mathrm{p})^3\mathrm{H}$, destroyed the deuterium nuclei just created. The overall primordial deuterium abundance is thus determined by the values of all these cross sections, experimentally determined in nuclear laboratories since the middle of last century. The related uncertainties changed in the last decades maintaining, however, the $^2\mathrm{H}(\mathrm{p},\gamma)^3\mathrm{He}$ reaction as the main source of error in the primordial deuterium abundance BBN calculation [18,26,27].

LUNA measured the $^2\mathrm{H}(\mathrm{p},\gamma)^3\mathrm{He}$ reaction in the Solar Gamow peak ($2.5\,\mathrm{keV} < E < 22\,\mathrm{keV}$) in 2002 [11], far away from the BBN energy range ($52\,\mathrm{keV} < E < 252\,\mathrm{keV}$ [28]). However, the new LUNA data definitely clarified the situation in the low energy range where previous experimental results differed by more than 50% [29]. Moreover, the inclusion of the new LUNA data increased the accuracy of the S-factor parametrization, when compared to previous analyses [30]. The available experimental data before and after LUNA are reported in fig. 2.

In 2002, high-precision Cosmic Microwave Background (CMB) measurements like those provided by WMAP [38] in 2003 and PLANCK [3] in 2015 were not available and thus BBN calculations of primordial deuterium abundance based on astronomical observations and nuclear cross section data were used to constrain cosmological parameters such as the baryon density Ω_b or the effective neutrino number N_{eff}. In this respect, the $^2\mathrm{H}(\mathrm{p},\gamma)^3\mathrm{He}$ was considered a cosmological baryometer.

Using the new evaluation of the $^2\mathrm{H}(\mathrm{p},\gamma)^3\mathrm{He}$ reaction rate improved with the LUNA data [30] and the high-precision baryon density value measured at WMAP [38], a primordial deuterium abundance with a precision comparable with the astronomical observations available at that time was obtained [30]. Thus, for the first time, astronomical observations on primordial deuterium could be compared with the BBN expected value. A small inconsistency between the measurements and the model prediction was found and later confirmed also by PLANCK [3,18].

Recently, new astronomical observations [5] reduced the uncertainty on the deuterium abundance to a 1.6% level, lower than the one obtained using BBN. The more recent values of the primordial deuterium abundance observed [5] and calculated [18] are reported in table 1.

The main source of error on the BBN value is the uncertainty on the $^2\mathrm{H}(\mathrm{p},\gamma)^3\mathrm{He}$ reaction rate, substantially due to the lack of experimental data points in the BBN region of interest [18]. Up to now, only Ma *et al.* [35] data are available in that energy range. A new experimental campaign devoted to a high-precision measurement of the $^2\mathrm{H}(\mathrm{p},\gamma)^3\mathrm{He}$ cross section is planned at LUNA in 2016.

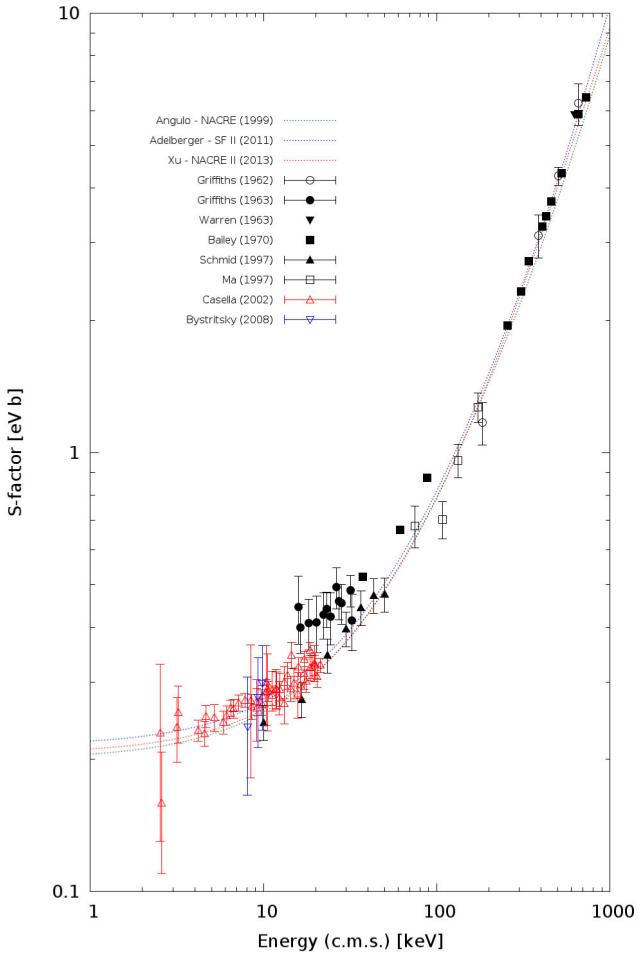

Fig. 2. Experimental data available before LUNA (black): Griffins *et al.* (1962) [31] and (1963) [32], Warren *et al.* (1963) [33], Bailey *et al.* (1970), Schmid *et al.* (1997) [34] and Ma *et al.* (1997) [35]. Experimental data available after LUNA (blue): Bystritsky (2008). LUNA (2002) data are indicated with red empty triangles [11]. Fit curves by NACRE I [36] and II [37] compilations and Adelberger [29] are also reported.

2.2 ^{3}He(^{2}H, p)^{4}He

The ^{3}He primordial abundance is mainly determined by the ^{3}He(^{2}H, p)^{4}He process and, to a lower extent, by the ^{2}H(p, γ)^{3}He reaction [39]. Both reactions were studied at LUNA but unfortunately outside the energy region of interest for BBN. Differently from the ^{2}H(p, γ)^{3}He case, discussed in details in sect. 2.1, the LUNA [12,13] data for the ^{3}He(^{2}H, p)^{4}He reaction did not considerably increase the precision of the ^{3}He primordial abundance estimation. Moreover, it is very difficult to measure the ^{3}He primordial abundance from the astronomical point of view given that this isotope is created and destroyed during the stellar/galactic evolution. This explains why ^{3}He was never used in the past as a cosmological baryometer due to the huge uncertainty on its observed value [40]. Experimental LUNA data points were used to calculate the ^{3}He primordial abundance [6,37]: the more recent value is reported in table 1.

2.3 ^{3}He(α, γ)^{7}Be

Lithium is the heaviest of the three elements predominantly produced in Big Bang nucleosynthesis (BBN). It has two stable isotopes, ^{7}Li (terrestrial abundance 92.5%, this section), and ^{6}Li (terrestrial abundance 7.5%, subsequent section). While ^{7}Li has long been believed to be produced mainly in Big Bang nucleosynthesis, it is assumed that ^{6}Li originates mainly in cosmic rays [41].

Ever since the discovery of the Spite plateau of lithium abundances in metal-poor halo stars [20], it has been a puzzle why standard BBN predicts a significantly higher amount of ^{7}Li than what is observed in primitive stars. With the recent very precise determination of the baryon-to-photon ratio based on the cosmic microwave background [3], this puzzle has only become more acute. BBN ^{7}Li predictions are now a factor of four higher than observations [21].

Recent data on very old stars at ultra-low metallicity [42,43] show an even stronger depletion of the lithium level, suggesting that the Spite plateau is no longer valid for these extreme cases. However, despite some scatter in lithium values, in none of these very old stars lithium abundances above the Spite plateau have been found. So the basic quandary that BBN predictions lie above the Spite plateau remains even for these below-Spite stars.

Astrophysical solutions to the ^{7}Li puzzle that are being discussed include diffusion inside stars that may dilute their ^{7}Li content [44]. Recently, a ^{7}Li abundance that is consistent with BBN predictions has been observed in the low-metallicity gas of the Small Magellanic Cloud [45], adding a piece to the puzzle. More exotic suggested solutions of the ^{7}Li puzzle include the temporary shifting of neutrons to a mirror universe [46].

The BBN production of ^{7}Li is dominated by the ^{3}He(α, γ)^{7}Be reaction, with subsequent decay of radioactive ^{7}Be to ^{7}Li. The ^{3}H(α, γ)^{7}Li reaction, on the other hand, plays only a minor role in ^{7}Li production [2].

The ^{3}He(α, γ)^{7}Be reaction was studied at LUNA using two different experimental techniques: First, the cross section was determined based on the offline determination of the ^{7}Be activity created in the experiment. In a second step, also the promptly emitted γ-rays from the reaction were detected and analyzed. For three runs at different beam energies, both methods were used in parallel, allowing to check for possible systematic discrepancies between them. Just such a systematic discrepancy between activation and in-beam γ method had previously been suggested, giving rise to some uncertainty [47].

The setup consisted of a windowless ^{3}He gas target, with the pressure gradient maintained by differential pumping in three pumping stages (see also [48]). The ^{3}He gas from the exhaust of the pumps was collected, purified in a chemical getter and recirculated into the target. The buildup of impurities passing the getter, which mainly consisted of surviving nitrogen, was monitored using the particle spectra from double elastic scattering of the ^{4}He$^+$ beam, firstly on the target gas (^{3}He and impurities), secondly on a carbon scattering foil to limit the scattered particle flux.

The beam intensity was determined with a beam calorimeter with constant temperature gradient [49] going from 70 °C at the hot side to 0 °C at the cold side. With beam, the effective target density is reduced due to the beam heating effect [50], leading to an effective thinning of the gas due to the heat deposited by the beam. This effect was studied with an elastic scattering device, giving the effective target density with 1.5% uncertainty [51].

For the activation method, the detection efficiency is given by the product of the efficiency to catch created ^{7}Be nuclei and the efficiency of the offline counting. For ^{7}Be created in the main gas target chamber, the geometric detection efficiency of the primary ^{7}Be catcher, consisting of a copper cap mounted on the calorimeter hot side, is 100% due to the kinematic forward focusing of the reaction products. However, some ^{7}Be nuclei are elastically backscattered from the copper surface of the catcher. This effect was studied in a GEANT4 [52] simulation and by experiment. Experimentally, an aluminium foil was mounted on the sides of the target chamber, forming a secondary catcher for backscattered ^{7}Be. Indeed, as predicted by the simulations, a tiny ^{7}Be activity of 0.8 mBq was found on the aluminium foil, detectable only in the very low background setting of the Gran Sasso deep underground γ-counting facility [53].

Further collection losses may occur if ^{7}Be is created not inside the main target chamber, but already in the low-pressure gas tube leading up to it or inside the narrow, 40 mm long collimator separating tube and main target chamber. Again, this effect was simulated and a specially prepared collimator catcher was mounted, showing a correction of 6.8 mBq for an experiment with 316 mBq activity detected on the main catcher. The precise knowledge of these two corrections was crucial for the final precision attained.

Due to the low ^{7}Be activities of always less than 1 Bq, the activated catchers had to be counted in very close geometry, just a few mm above the endcap of the ultra low background high-purity germanium (HPGe) detector. In this geometry, it is very difficult to precisely calibrate the detection efficiency. Therefore, dedicated ^{7}Be calibration sources in the 100 Bq activity range were created, their activity was determined in far geometry based on ^{137}Cs, ^{60}Co, and ^{22}Na sources, and then they were used to calibrate the detector in close geometry. With this method, simulation based corrections could be minimized, and the counting efficiency was determined to $\pm 1.8\%$. The branching ratio for the emission of the 478 keV γ-ray in ^{7}Be decay is very precisely known, $(10.44 \pm 0.04)\%$ [54].

Based on these considerations, the final systematic uncertainty in the cross section determined by the activation method was 3.0% [14–16]. The in-beam γ-spectrometry data had a slightly higher systematic uncertainty of 3.6% due to the unknown γ-ray angular distribution [16]. The new LUNA data (fig. 3) are lower in energy than ever before, so that now the entire sensitive energy region for BBN is covered with experimental data.

The experimental and theoretical situation in the ^{3}He$(\alpha,\gamma)^7$Be reaction at $E > 1$ MeV has recently attracted much attention. This is so because at $E \approx 2$ MeV the modern di Leva data [57] were about 40% higher than the 50-year-old data by Parker and Kavanagh [63]. This conclusion [57] was subsequently confirmed in a number of recent experiments [58–60].

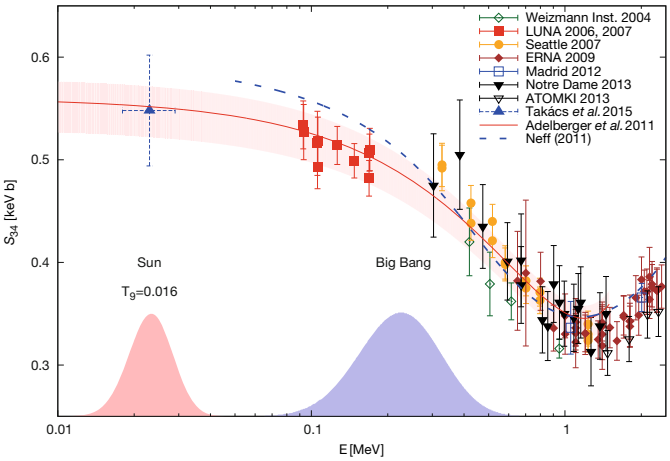

Fig. 3. Astrophysical S-factor of the ^{3}He$(\alpha,\gamma)^7$Be reaction from modern experiments [55–60] and from rescaling the ^{7}Be solar neutrino flux [61]. A theoretical curve rescaled to match the modern data [29], and *ab initio* theory [62] are given. The Gamow peak for the Sun and the sensitive energy region for BBN [61] have been added.

A direct comparison of the LUNA data with other works is difficult, because they do not overlap in energy. Any comparison needs to assume some energy dependence, for example that of the theretical curve used in the Adelberger *et al.* compilation [29]. When using this curve, it is found that the modern cross section measurements confirm the LUNA data, of course with some uncertainty due to the extrapolation to lower energies (fig. 3). An additional indirect confirmation that the LUNA data are correct was recently found by using the observed ^{7}Be neutrino flux and the standard solar model to extract the ^{3}He$(\alpha,\gamma)^7$Be cross section at the solar Gamow peak energy [61].

However, it is still highly desirable to extend the LUNA ^{3}He$(\alpha,\gamma)^7$Be data to both lower and higher energies, in order to firm up the comparison to high-energy overground data. Given this caveat, it can still be said that the LUNA ^{3}He$(\alpha,\gamma)^7$Be data rule out any nuclear solution to the BBN ^{7}Li problem. The predicted ^{7}Li production is much higher, $^7\mathrm{Li/H} = (5.1 \pm 0.4) \times 10^{-10}$ [9].

2.4 ^{2}H$(\alpha,\gamma)^6$Li

^{6}Li detection in astronomical objects such as the metal poor dwarf star HD 84937 in the Galactic halo [64,65] can be performed using the small isotopic effect on lithium absorption lines. Thus, a large number of stars has been surveyed for ^{6}Li in this way by Asplund *et al.* in the 2000 years, and significant values for the isotopic abundance ^{6}Li/^{7}Li have been found in about a dozen cases [10,66].

Table 2. Observations of ^{6}Li/^{7}Li isotopic abundances in two selected metal poor halo stars using two different methods: 1D LTE = one-dimensional model atmosphere, local thermal equilibrium assumed. 3D NLTE = three-dimensional model atmosphere, no local thermal equilibrium assumed.

Object	^{6}Li/^{7}Li [%]	Method	Reference
HD 84937	5 ± 2	1D LTE	[64]
	5.2 ± 1.9	1D LTE	[65]
	5.1 ± 2.3	3D NLTE	[68]
	1.7 ± 0.9	3D NLTE	[69]
G 64-12	5.9 ± 2.1	1D LTE	[66]
	0.8 ± 2.7	3D NLTE	[68]
	-0.2 ± 1.4	3D NLTE	[69]

However, other workers pointed out that by using three-dimensional model atmospheres and dropping the assumption of local thermal equilibrium these detections may become insignificant [67], with the notable exception of HD 84937 [68]. Very recently, Asplund *et al.* presented new data based on higher-quality observations and upgraded models [69] that rule out several of the previous ^{6}Li/^{7}Li detections including their own (table 2, for two examples).

If even one of the disputed ^{6}Li/^{7}Li detections, *e.g.* the one for HD 84937 [64,65,68], is confirmed, there remains the problem on how to produce ^{6}Li in very primitive stars without at the same time destroying all ^{7}Li. Contrary to the case of ^{7}Li (see previous section), there are no standard physics solutions proposed for the production of ^{6}Li. Standard BBN results in $^6\mathrm{Li}/^7\mathrm{Li} = (2 \pm 3) \cdot 10^{-5}$ [2], much below the detected levels. As a possible solution, it has been suggested that both stable lithium isotopes may be created in the hot tori formed around stellar black holes, but this interesting possibility actually worsens the ^{7}Li puzzle while solving the ^{6}Li one [70]. More exotic possible solutions include catalysis by long-living particles not included in the standard model [22,23] and non-equilibrium BBN [24].

Standard BBN production of ^{6}Li is dominated by just one nuclear reaction, $^2\mathrm{H}(\alpha,\gamma)^6\mathrm{Li}$ [2]. This reaction has been studied before LUNA (fig. 4): by detection of the ^{6}Li residual nucleus [71], by in-beam γ-spectroscopy at the $E = 0.711$ MeV resonance[1] [72], and in two separate Coulomb dissociation experiments at 26 [73] and 150 MeV/nucleon [75] ^{6}Li projectile energy, respectively. The first Coulomb dissociation experiment reported positive $^2\mathrm{H}(\alpha,\gamma)^6\mathrm{Li}$ cross section values [73]. However, the higher-energy, second work reported such a high background from nuclear breakup that no $^2\mathrm{H}(\alpha,\gamma)^6\mathrm{Li}$ cross section could be extracted [75], an effect that should affect the lower-energy data [73] even more strongly. Therefore, these data [73] have to be interpreted as upper limits. The higher-energy Coulomb dissociation work [75] reports a theoretical excitation function that is to some extent corroborated by the reconstructed angular distribution of

[1] In the following, E refers to the center-of-mass energy and E_α to the ^{4}He projectile energy in the laboratory system.

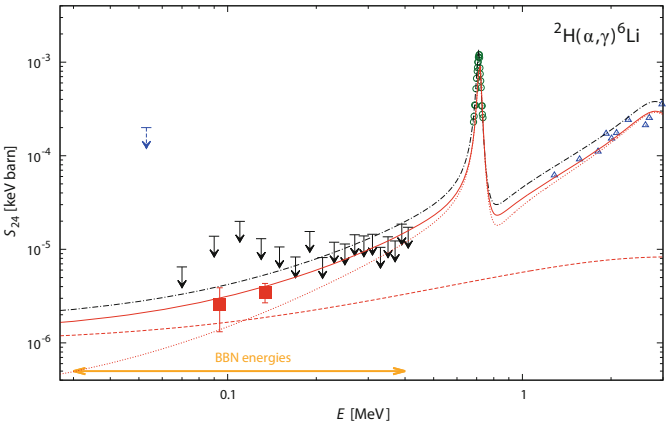

Fig. 4. Astrophysical S-factor of the $^2\mathrm{H}(\alpha,\gamma)^6\mathrm{Li}$ reaction, from the literature (data: blue triangles [71], green circles [72]; upper limits: black arrows [73], blue dashed arrow [74]; theory black dot-dashed curve [75]) and from LUNA (red squares [9]). The red curves (full = total, short-dashed = $E2$, long-dashed = $E1$) are the previous theory curve [75], rescaled to match the present data.

the excited ^{6}Li nuclei. A separate attempt to directly measure the $^2\mathrm{H}(\alpha,\gamma)^6\mathrm{Li}$ cross section in the Big Bang energy range by in-beam γ spectroscopy resulted only in an upper limit [74].

In order to resolve the conflicting data situation, at LUNA the $^2\mathrm{H}(\alpha,\gamma)^6\mathrm{Li}$ S-factor was measured directly at astrophysically relevant energies, where the $^2\mathrm{H}(\alpha,\gamma)^6\mathrm{Li}$ reaction (Q-value 1.474 MeV) proceeds via direct capture directly to the ground state of ^{6}Li and emits a single γ-ray of energy $E_\gamma = Q + E$, either via electric dipole ($E1$) or electric quadrupole ($E2$) capture. The cross section is very small (about 60 pbarn at $E = 133$ keV) and, well below the Coulomb barrier, strongly dependent on E. To measure the cross section directly and with a sufficient precision, the following issues had to be properly faced:

1) The need of a high signal-to-noise ratio to avoid big statistical errors which are expected to dominate if only few events can be detected.

2) The necessity of a precise knowledge of the energy at which the reaction occurs. For this reason, solid targets (*e.g.* deuterated metals) are not useful due to a rapid stopping of incident particles inside the upper target layers, leaving E uncertain. Secondly, the stability of such a target would be affected by the high temperatures at the beam spot, leading to a highly uncertain target density. Hence, a windowless gaseous target is preferable: in this way constantly renewed and stable conditions can be obtained.

The setup used for the LUNA measurement is shown in fig. 5. The emitted γ-rays of the $^2\mathrm{H}(\alpha,\gamma)^6\mathrm{Li}$ reaction were detected by an ultra-low background high-purity germanium detector with a high relative efficiency of 137%. The detector was located as close as possible to the beam (distance to the surface of the detector window: 15 mm). The setup was fully surrounded by at least 20 cm of lead and

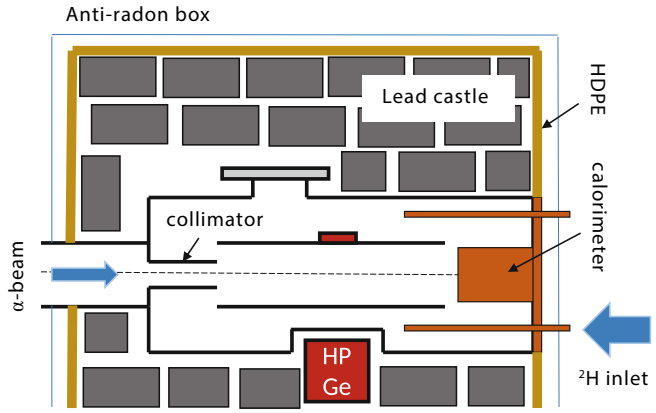

Fig. 5. Setup used at LUNA for the ^{2}H$(\alpha,\gamma)^6$Li cross section measurement campaign. More details are reported in [76,77].

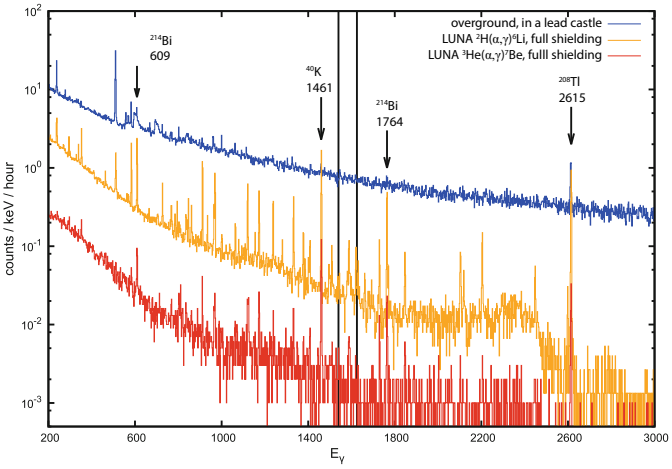

Fig. 6. Laboratory background in the LUNA setups for the study of the reactions for BBN lithium production: ^{3}He$(\alpha,\gamma)^7$Be setup with Pb and Cu shield (red curve, [16]), ^{2}H$(\alpha,\gamma)^6$Li setup with Pb shield but no Cu (orange curve, [9]). For comparison, a spectrum at the surface of the Earth in a fully closed 15 cm thick Pb+Cu graded shield is shown (blue curve, [76]).

enclosed in an anti-radon box flushed with pure nitrogen to maintain a stable low natural background rate (fig. 6).

The output of the HPGe detector was processed by a fast digitizer module, the events were stored along with their timestamp. In this way, periods with an increased noise could be discarded later.

The energy of the ^{2}H$(\alpha,\gamma)^6$Li γ-rays depends on the Q value of the reaction and on the beam energy E_α. The region of interest is stretched (up to 35 keV at $E_\alpha = 400$ keV) by a large Doppler shift correction due to the close detector geometry. Hence, a weak signal is distributed within a comparably large γ energy range. In addition, deuterons scattered by incident ^{4}He$^+$ ions may interact with other deuterons via the ^{2}H$(^2$H, n$)^3$He reaction, creating a low (about 10 s^{-1}) but steady neutron flux. The neutrons interact with the detector as well as with the setup materials, creating a beam induced background which exceeds the ^{2}H$(\alpha,\gamma)^6$Li γ signal in the region of

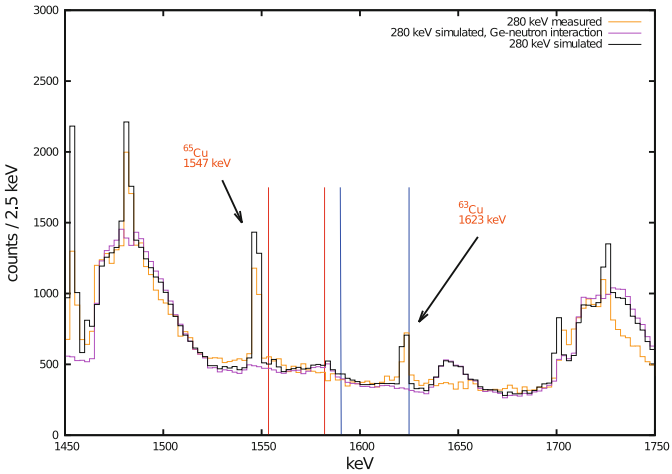

Fig. 7. Measured data at a beam energy of $E_\alpha = 280$ keV (orange curve) compared to arbitrarily normalized spectra obtained from a GEANT4 simulation: The contribution to the beam induced background due to the interaction of neutrons with the HPGe crystal (magenta) and the full simulated spectrum (black), adding mainly the effect of neutron interaction with surrounding materials (*e.g.* copper). The ^{2}H$(\alpha,\gamma)^6$Li regions of interest are marked with red ($E_\alpha = 280$ keV) and blue ($E_\alpha = 400$ keV) lines.

interest (1590 keV $< E_\gamma <$ 1625 keV at $E_\alpha = 400$ keV) by a factor of more than ten. Hence, the experimental setup and the measurement conditions needed to be optimized, and methods to subtract the beam induced background had to be developed.

In general, the ^{2}H$(\alpha,\gamma)^6$Li setup was a modified version of the previous ^{3}He$(\alpha,\gamma)^7$Be setup, still being a windowless gas target and using a very similar beam calorimeter. The deuterium pressure in the target was optimized to 0.3 mbar. The well collimated ^{4}He$^+$ beam (with a typical intensity of 0.3 mA) interacted with the gas target on a range of 17.6 cm, surrounded by a steel tube to limit the path of scattered deuterons. With these parameters, a typical rate for detecting γ-rays from ^{2}H$(\alpha,\gamma)^6$Li reaction of about 2 h^{-1} ($E_\alpha = 400$ keV) could be expected. For the ^{2}H$(\alpha,\gamma)^6$Li measurement, the 5 cm thick inner copper lining of the shield had to be sacrificed, in order to reduce neutron induced γ-rays in copper. This led to a somewhat higher no-beam background (1.2 events per hour in the 400 keV region of interest); however still orders of magnitude below the background in well-shielded setups at the surface of the Earth (fig. 7).

The beam-induced background generated by the neutron flux increases the background continuum in the γ spectrum in general. In addition, distinct lines from (n, n$'\gamma$) interactions on setup materials as well as large triangular structures from such interactions inside the Ge crystal can be found (see [77] for a discussion). The beam-induced background inside the ^{2}H$(\alpha,\gamma)^6$Li region of interest at $E_\alpha = 400$ keV is mainly flat, touched by a ^{63}Cu(n, n$'\gamma$) line at the right edge (see fig. 7). The beam-induced background could be well reproduced by a GEANT 4 simulation [77] which allowed to study the

contribution of several interaction processes. Due to the high Q-value of the ^{2}H(^{2}H, n)^{3}He reaction, the neutron energy is almost independent of E_α. Hence, the shape of the beam induced background is nearly independent of the beam energy. This allows to reproduce the background using a lower beam energy (*e.g.* $E_\alpha = 280\,\mathrm{keV}$), with a region of interest shifted to lower γ energies (fig. 7). Subtracting such spectra should eliminate the beam-induced background, leaving the two signals behind. Several data sets at beam energies of $E_\alpha = 240\,\mathrm{keV}$, 280 keV, 360 keV and 400 keV with a summed beam charge of more than 1 kCoulomb have been collected, corresponding to center-of-mass energies of 80 keV, 93 keV, 120 keV and 133 keV.

In reality, the beam-induced background has a small dependence on E_α, so several corrections to a simple subtraction had to be applied [76]. Two indepent approaches were developed: In a first approach, the correct normalization function was obtained by a χ^2 minimization routine using the 1500–1625 keV range in the γ spectrum [9]. In another approach, the flat background continuum was parameterized using regions without distinct peaks along the entire γ spectrum. Both methods yielded consistent results [9,78]. The main contribution to the uncertainty is the statistical error [9,76,78] due to the subtraction of big numbers.

In fig. 4, the LUNA S-factors for the two energies 93 and 133 keV are shown together with previous direct and indirect measurements. A full data analysis including also the 80 and 120 keV energies will be available soon [78]. The first direct measurement in the Big Bang energy region provides slightly lower values than reported from the recent indirect measurement using the nuclear breakup method. As in the case of the ^{3}He$(\alpha,\gamma)^7$Be reaction, also for ^{2}H$(\alpha,\gamma)^6$Li it would be relevant to connect the low-energy LUNA data to direct cross section measurements at the surface by data over a wide energy range. This would require a higher-energy underground accelerator, such as LUNA-MV.

The resulting lithium isotopic ratio from BBN, based on the LUNA experiments on ^{3}He$(\alpha,\gamma)^7$Be for ^{7}Li [79] and ^{2}H$(\alpha,\gamma)^6$Li for ^{6}Li, is $^6\mathrm{Li}/^7\mathrm{Li} = (1.5 \pm 0.3) \cdot 10^{-5}$, to be compared with $^6\mathrm{Li}/^7\mathrm{Li} = 2.4 \cdot 10^{-5}$ from CF88 [80], and with $(2 \pm 3) \cdot 10^{-5}$ from the Naples Big Bang code [2]. The LUNA experiment-based ^{6}Li/^{7}Li isotopic abundance ratio is much lower than the terrestrial ratio of $0.075/0.925 = 0.081$. The LUNA data firmly ruled out BBN production as a possible explanation for the disputed ^{6}Li detections in metal-poor stars.

Pre-galactic ^{6}Li production mechanisms have previously been ruled out as a possible explanation ([81] and references therein). Local production of ^{6}Li by stellar flares using the ^{4}He(^{3}He,p)^{6}Li reaction has been proposed as a possible solution [82], but this scenario would require special conditions to be true in all stars with ^{6}Li observations. As a result, the only remaining scenarios explaining a global ^{6}Li/^{7}Li level of a few percent as detected [10,64–66,68] involve non-standard physics [22–24]. Cosmic ^{6}Li is clearly a highly interesting probe of physics beyond the standard model.

3 Future outlook

Big Bang nucleosynthesis is the natural connection between nuclear physics and cosmology. In the last decades, a constructive loop between these two fields of physics provided either prediction of primordial abundances or constraints on the cosmological model parameters. The choice depends on the accuracy achieved either in cosmological or nuclear physics experiments. Before WMAP, nuclear cross section measurements provided constraints on baryon density. LUNA contributed to this process measuring some key reactions for BBN like the ^{2}H$(\mathrm{p},\gamma)^3$He, ^{3}He$(^2\mathrm{H},\mathrm{p})^4$He and ^{3}He$(\alpha,\gamma)^7$Be described in this paper. Starting from the beginning of this century, thanks to the high-precision Cosmic Microwave Background radiation measurements provided by WMAP and PLANCK, the cosmological parameters obtained from the data analysis were used to calculate the primordial abundances of light elements. In the Standard Model with three neutrino families, BBN makes relatively accurate predictions except for lithium. In the case of the ^{6}Li isotope, the discrepancy between calculations and astronomical observations was assigned to the lack of knowledge in the cross section of the leading process for ^{6}Li primordial production: the ^{2}H$(\alpha,\gamma)^6$Li. This reaction was directly measured for the first time at LUNA. LUNA data ruled out any nuclear solution to the ^{6}Li problem. The same result has been obtained for ^{7}Li also thanks to the new low-energy cross section data obtained at LUNA for the ^{3}He$(\alpha,\gamma)^7$Be reaction. The discrepancy between BBN calculations and astronomical observations for lithium, the so-called "lithium problem", could provide new constraints on the cosmological parameters especially if extensions of the ΛCDM model are considered. However, the primordial nature of the lithium observed is still debated. The situation is clearer for deuterium since its primordial abundance has a clear signature from the astronomical point of view. Thus, a high-precision measurement of the ^{2}H$(\mathrm{p},\gamma)^3$He cross section at LUNA in the BBN energy range, planned for 2016, could provide new constraints on cosmological parameters.

Moreover, LUNA-MV will be able to directly measure the ^{3}He$(\alpha,\gamma)^7$Be reaction in the BBN energy range [79] where the quality of the data are poor and to refine the knowledge of the ^{2}H$(\alpha,\gamma)^6$Li cross section between the actual low energy LUNA data and the other measurements taken at high energies.

In conclusion, the high accuracy reached by the CMB and nuclear cross section measurements goes in the direction of a new era of Physics: the so-called "Nuclear Cosmology". The consistency between the cosmological model (with its parameters and reaction rates) and the primordial abundances observed should be preserved to obtain a consistent framework. Precise astronomical observations are thus a key-point for the future. From the nuclear side, LUNA could investigate BBN reactions in their appropriate energy range. The low background of LNGS as well as the experience acquired in the last decades by the LUNA collaboration could give a unique possibility to obtain a real development of the "Nuclear Cosmology" opening new doors in the direction of New Physics.

References

1. F. Iocco *et al.*, Phys. Rep. **472**, 176 (2009).
2. P.D. Serpico *et al.*, J. Cosmol. Astropart. Phys. **2004**, 010 (2004).
3. P.A.R. Ade *et al.*, arXiv:1502.01589 (2015).
4. Y.I. Izotov *et al.*, Astron. Astrophys. **558**, A57 (2013).
5. R.J. Cooke *et al.*, Astrophys. J. **781**, 31 (2014).
6. R.H. Cyburt *et al.*, arXiv:1505.01076v1 (2015).
7. T. Bania *et al.*, Nature **415**, 54 (2002).
8. S.G. Ryan *et al.*, Astrophys. J. Lett. **530**, L57 (2000).
9. M. Anders *et al.*, Phys. Rev. Lett. **113**, 042501 (2014).
10. M. Asplund *et al.*, Astrophys. J. **644**, 229 (2006).
11. C. Casella *et al.*, Nucl. Phys. A **706**, 203 (2002).
12. H. Costantini *et al.*, Phys. Lett. B **482**, 43 (2000).
13. M. Aliotta *et al.*, Nucl. Phys. A **690**, 790 (2001).
14. D. Bemmerer *et al.*, Phys. Rev. Lett. **97**, 122502 (2006).
15. Gy. Gyürki *et al.*, Phys. Rev. C **75**, 035805 (2007).
16. F. Confortola *et al.*, Phys. Rev. C **75**, 065803 (2007).
17. H. Costantini *et al.*, Nucl. Phys. A **814**, 144 (2008).
18. E. Di Valentino *et al.*, Phys. Rev. D **90**, 023543 (2014).
19. K.M. Nollett, G.P. Holder, arXiv:1112.2683v1 (2011).
20. M. Spite, F. Spite, Nature **297**, 483 (1982).
21. B.D. Fields, Annu. Rev. Nucl. Part. Sci. **61**, 47 (2011).
22. K. Jedamzik, M. Pospelov, New J. Phys. **11**, 105028 (2009).
23. H. Dapo *et al.*, Phys. Rev. C **85**, 044602 (2012).
24. M. Pospelov, J. Pradler, Annu. Rev. Nucl. Part. Sci. **60**, 539 (2010).
25. M. Kusakabe *et al.*, Phys. Rev. D **76**, 121302 (2007).
26. L.M. Krauss, P. Romanelli, Astrophys. J. **358**, 47 (1990).
27. R.H. Cyburt *et al.*, New Astron. **6**, 215 (2001).
28. S. Burles *et al.*, Phys. Rev. Lett. **82**, 4176 (1999).
29. E.G. Adelberger *et al.*, Rev. Mod. Phys. **83**, 195 (2011).
30. R.H. Cyburt, Phys. Rev. D **70**, 023505 (2004).
31. G.M. Griffiths *et al.*, Can. J. Phys. **40**, 402 (1962).
32. G.M. Griffiths *et al.*, Can. J. Phys. **41**, 724 (1963).
33. J.B. Warren *et al.*, Phys. Rev. **132**, 1691 (1963).
34. G.J. Schmid *et al.*, Phys. Rev. C **56**, 2565 (1997).
35. L. Ma *et al.*, Phys. Rev. C **55**, 588 (1997).
36. C. Angulo *et al.*, Nucl. Phys. A **656**, 3 (1999).
37. Y. Xu *et al.*, Nucl. Phys. A **918**, 61 (2013).
38. D.N. Spergel *et al.*, Astrophys. J. Suppl. Ser. **148**, 175 (2003).
39. A. Coc *et al.*, J. Cosmol. Astropart. Phys. **2014**, 50 (2014).
40. E. Vangioni-Flam *et al.*, Astron. Astrophys. **360**, 15 (2000).
41. D.D. Clayton, *Handbook of Isotopes in the Cosmos: Hydrogen to Gallium* (Cambridge University Press, Cambridge, 2003).
42. L. Sbordone *et al.*, Astron. Astrophys. **522**, A26 (2010).
43. E. Caffau *et al.*, Nature **477**, 67 (2011).
44. A.J. Korn *et al.*, Nature **442**, 657 (2006).
45. J.C. Howk *et al.*, Nature **489**, 121 (2012).
46. A. Coc *et al.*, Phys. Rev. D **87**, 123530 (2013).
47. E. Adelberger *et al.*, Rev. Mod. Phys. **70**, 1265 (1998).
48. A. Formicola *et al.*, Eur. Phys. J. A **52**, 73 (2016) contribution to this Topical Issue.
49. C. Casella *et al.*, Nucl. Instrum. Methods A **489**, 160 (2002).
50. J. Görres *et al.*, Nucl. Instrum. Methods A **177**, 295 (1980).
51. M. Marta *et al.*, Nucl. Instrum. Methods A **569**, 727 (2006).
52. S. Agostinelli *et al.*, Nucl. Instrum. Methods A **506**, 250 (2003).
53. C. Arpesella, Appl. Radiat. Isot. **47**, 991 (1996).
54. D. Tilley *et al.*, Nucl. Phys. A **708**, 3 (2002).
55. B. Nara Singh *et al.*, Phys. Rev. Lett. **93**, 262503 (2004).
56. T.A.D. Brown *et al.*, Phys. Rev. C **76**, 055801 (2007).
57. A. di Leva *et al.*, Phys. Rev. Lett. **102**, 232502 (2009).
58. M. Carmona-Gallardo *et al.*, Phys. Rev. C **86**, 032801 (2012).
59. C. Bordeanu *et al.*, Nucl. Phys. A **908**, 1 (2013).
60. A. Kontos *et al.*, Phys. Rev. C **87**, 065804 (2013).
61. M.P. Takács *et al.*, Phys. Rev. D **91**, 123526 (2015).
62. T. Neff, Phys. Rev. Lett. **106**, 042502 (2011).
63. P. Parker, R. Kavanagh, Phys. Rev. **131**, 2578 (1963).
64. V.V. Smith *et al.*, Astrophys. J. **408**, 262 (1993).
65. R. Cayrel *et al.*, Astron. Astrophys. **343**, 923 (1999).
66. M. Asplund, J. Meléndez, AIP Conf. Proc. **990**, 342 (2008).
67. P. Bonifacio *et al.*, Astron. Astrophys. **462**, 851 (2007).
68. M. Steffen *et al.*, Mem. Soc. Astron. Ital. **22**, 152 (2012).
69. K. Lind *et al.*, Astron. Astrophys. **554**, A96 (2013).
70. F. Iocco, M. Pato, Phys. Rev. Lett. **109**, 021102 (2012).
71. R.G.H. Robertson *et al.*, Phys. Rev. Lett. **47**, 1867 (1981).
72. P. Mohr *et al.*, Phys. Rev. C **50**, 1543 (1994).
73. J. Kiener *et al.*, Phys. Rev. C **44**, 2195 (1991).
74. F.E. Cecil *et al.*, Phys. Rev. C **53**, 1967 (1996).
75. F. Hammache *et al.*, Phys. Rev. C **82**, 065803 (2010).
76. M. Anders, *S-factor measurement of the* $^2\mathrm{H}(\alpha,\gamma)^6\mathrm{Li}$ *reaction at energies relevant for Big-Bang nucleosynthesis*, Report HZDR-042 (2013) and PhD Thesis, Technical University of Dresden (2013).
77. M. Anders *et al.*, Eur. Phys. J. A **49**, 28 (2013).
78. D. Trezzi *et al.*, submitted to Part. Phys.
79. M. Aliotta *et al.*, *Helium burning and neutron sources in stars*, contribution to this Topical Issue.
80. G.R. Caughlan, W.A. Fowler, At. Data Nucl. Data Tables **40**, 283 (1988).
81. N. Prantzos, Astron. Astrophys. **542**, A67 (2012).
82. V. Tatischeff, J.-P. Thibaud, Astron. Astrophys. **469**, 265 (2007).